Two-dimensional scanning capacitance microscopy measurements of cross-sectioned very large scale integration test structures

Gabi Neubauer and Andrew Erickson[a)]
Materials Technology Department, Intel Corporation, Santa Clara, California 95052

Clayton C. Williams
Department of Physics, University of Utah, Salt Lake City, Utah 84105

Joseph J. Kopanski
National Institute of Standards and Technology, Gaithersburg, Maryland 20899

Mark Rodgers and Dennis Adderton
Digital Instruments, Santa Barbara, California 93103

(Received 3 February 1995; accepted 20 October 1995)

Scanning probe technology, with its inherent two-dimensionality, offers unique capabilities for the measurement of electrical properties on a nanoscale. We have developed a setup which uses scanning capacitance microscopy (SCM) to obtain electrical information of cross-sectioned samples while simultaneously acquiring conventional topographical atomic force microscopy (AFM) data. In an extension of our work on very large scale integration cross sections, we have now obtained one-dimensional and two-dimensional SCM data of cross sections of blanket-implanted, annealed Si wafers as well as special test structures on Si. We find excellent agreement of total implant depth obtained from SCM signals of these cross-sectioned samples with conventional secondary ion mass spectrometry (SIMS) profiles of the same samples. Although no modeling for a direct correlation between signal output and absolute concentration has yet been attempted, we have inferred quantitative dopant concentrations from correlation to SIMS depth profiles obtained on the same sample. By these means of indirect modeling, we have found that our SCM technique is sensitive to carrier density concentrations varying over several orders of magnitude, i.e., $<1\times10^{15}$ to 1×10^{20} atoms/cm^3, with a lateral resolution of 20–150 nm, depending on tip and dopant level.

I. INTRODUCTION

Over the last few years, an increasing need has been identified for direct two-dimensional measurement of carrier densities in semiconductor devices to provide a means for the calibration of process modeling. Up until now, quantitative two-dimensional information could only be inferred from one-dimensional dopant/carrier level measurements via secondary ion mass spectroscopy (SIMS), spreading resistance profilometry (SRP), and capacitance–voltage ($C-V$) measurements. A variety of different approaches have been taken to close this gap experimentally.[1] These include development of different staining or etching procedures which are sensitive to concentration and type of electrically active dopants.[1–3] Also, certain SIMS applications, such as angle lapping and employment of tomography techniques, allow us to calculate and display two-dimensional chemical dopant distributions from a multitude of one-dimensional measurements.[4,5] Often, these techniques provide only an indirect measurement of carrier densities and/or require lengthy sample preparations. The development of methods to measure electrical properties, which are suitable to directly yield the desired carrier distributions on a submicron scale, has greatly benefited from the development of scanning probe technology over the last decade. This technique offers inherent two-dimensionality. Derivatives of both the principal scanning probe techniques, i.e., scanning tunneling microscopy (STM) and atomic force microscopy (AFM), have been applied. STM measurements of chemically etched Si surfaces have been reported,[6] but most STM-based applications concentrate on work-function measurements. Significant progress has been made for Si-based structures[7–12] as well as for composite III–V semiconductors where single atom dopant imaging has been reported.[12–18] Purely STM and displacement current based concepts require conductive (or semiconductive) surface properties; hence, an application to complex very large scale integration (VLSI) structures of a largely nonconductive nature proves very difficult. In addition, spatial correlation of electrical measurements to specific points within the device geometry is difficult as well, since no independent input of topographical data is available. These problems can be overcome when the setup is implemented into an AFM which is equipped with a conductive tip/cantilever assembly to allow electrical measurements. Topographical AFM imaging generally occurs in repulsive mode, i.e., with contact between tip and sample. Consequently, detection mechanisms for electrical properties other than tunneling have to be pursued to avoid the necessity for an air or vacuum gap. Research in this area has mostly concentrated on developing setups feasible to measure

[a)]Present address: Digital Instruments, Santa Barbara, CA 93103.

capacitance,[19–25] spreading resistance,[26–29] and contact potential using a Kelvin probe setup.[30] Recently, one-dimensional and two-dimensional dopant profiles have been successfully measured by registering the spreading resistance between a conductive AFM tip and the sample while scanning.[26] This technique combines the classical, well known SRP technique with scanning probe technology. Although measurement stability was found to be sensitive to the applied load on the probe tip, a sensitivity of 1×10^{14} to 1×10^{19} atoms/cm^3 has been found under stable operation.

We have seen a similar advantage in evaluating scanning capacitance microscopy (SCM) for its capability to deliver two-dimensional carrier density information. We have chosen this technique, because $C-V$ measurements in one dimension already are a standard procedure in semiconductor characterization. The knowledge gained in that field will aid in the understanding of two-dimensional measurements and ultimately lead to directly measured local carrier densities in two dimensions. Our article presents our SCM application in an AFM setup to measure relative capacitance changes when scanning cross-sectioned implanted Si wafers and test structures on silicon. Earlier experiments had shown the AFM to be capable of imaging VLSI cross sections.[31] A contrast in AFM images of polished VLSI cross sections is due to the topography which develops from the material-dependent removal rates during polishing. In our new setup this topographical information is acquired simultaneously with the electrical data and is used to spatially correlate the data.

II. EXPERIMENTAL SETUP

Our experiments are conducted on a Digital Instruments Nanoscope III Large-Stage AFM, operated in air. Topography information is obtained with the probe tip scanning under constant repulsive force via a feedback network which maintains a load of approximately 5×10^{-7} N. The tip and part of the cantilever substrate are coated with chromium of a thickness of 300–500 Å. In initial setups, we had relied on the thin native oxide layer on the sample to serve as a thin insulator between coated tip and sample. However, this thin oxide layer was not sufficient to prevent the onset of tunneling current at bias voltages larger than a few volts. We have therefore now obtained better insulating properties when using a double coating on the tip consisting of ~400 Å chromium, followed by a SiO_2 layer of ~100–150 Å.

Capacitance measurements are accomplished by an RCA capacitance sensor circuitry which was originally designed for the RCA Video disk player.[32] Its operation is based on a 915 MHz oscillator driving a resonance circuit which is tuned in part by the external capacitance to be measured. As the resonant frequency is moved off the oscillator frequency by the external capacitance, the amplitude of the oscillation is decreased. The peak oscillation of the resonant circuit is detected and, after being rectified, forms the sensor output. An ac bias (typically 5–10 V, 10 kHz) is superimposed on a dc sample bias (2–3 V), while the tip is at virtual ground. The ac bias is chosen large enough to alternately deplete and accumulate the surface region, thus modulating the surface capacitance under the probe tip at the bias frequency. The RCA sensor output is then fed through a lock-in amplifier into the auxiliary input of the AFM, and topography and capacitance data are recorded simultaneously while the probe tip is raster-scanned across the surface. This setup scans the entire $C-V$ curve for each point on the x,y raster and acquires overall relative capacitance changes, ΔC_{rel}. Quite clearly, this setup does not allow us to extract any information which we could obtain when recording full $C-V$ curves. However, it is less dependent on shifts in the flat band voltage due to oxide or surface charges.

Sample preparation was optimized during our earlier experiments[31] similarly to the standard metallographic secondary electron microscopy cross-section preparation: a glass cover slide is attached to the specimen to protect the top layers; a sequence of grinding and polishing steps follows in which gradually higher grades of polishing papers are employed, ending with a final polishing step with a silica slurry. During these preparation steps, a native oxide is formed on the exposed cross-section surface. No attempts have been made at this point to further passivate the sample.

Although our setup is capable of detecting junctions,[33] we have decided here to concentrate on implant samples with no junctions. This is for the benefit of a more systematic approach to derive characteristic parameters of the technique, such as resolution, sensitivity, and general limitations. Two types of samples were used in this study. Initially, we used cross sections of blanket implanted and annealed Si wafers to evaluate the technique. Results included here were obtained from a p-type test wafer, implanted with boron at a dose of 1×10^{14} atoms/cm^2 at 100 keV. True two-dimensional data were obtained from a cross section of a special test structure which has been developed at NIST. In brief, the processing steps were as follows: A bulk doped p-type silicon substrate (about 1×10^{16} atoms/cm^3) obtained an oxide pattern (~8 nm thick) which served as a mask for a high dose implant of 1×10^{15} atoms/cm^2 of boron at 50 keV. A subsequent oxidizing step provided another 8 nm of oxide while simultaneously annealing the sample, resulting in a small step in the oxide at the implant edge. This process delivered stripes of lightly bulk-doped p-type Si, covered with ~16 nm of oxide, alternating with highly doped p-type Si, covered with ~8 nm of oxide. As we will discuss below, our results indicate that the masking might have been insufficient, causing the masked area to get implanted to some extent in the near-surface region. Cross sections were prepared by cutting through the line pattern to be able to take measurements at the exposed implanted area. The following section presents cross-sectional data obtained on both types of samples.

III. RESULTS

Figure 1 shows images acquired simultaneously on a cross section of a blanket Si-wafer implant of 1×10^{14} atoms/cm^2 of boron at 100 keV into a p-type substrate (3×10^{14} atoms/cm^3), scanned over an area of 3 μm$\times$1.5 μm. The topography image is at the top. In both images, the Si substrate is on the right-hand side. Brightness corresponds to

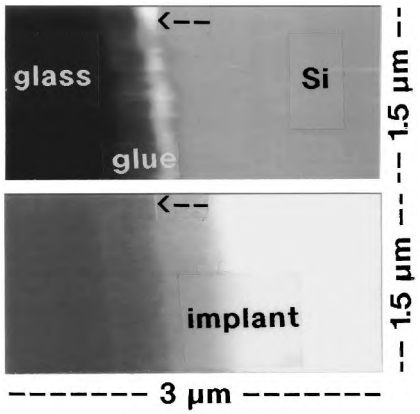

FIG. 1. Simultaneously acquired SCM (bottom) and topographical data (top) of a cross-sectioned blanket Si wafer implant (1×10^{14} atoms/cm^2 ^{11}B, 100 keV), scanned over an area of 3 μm×1.5 μm; signal ranges are 20 V and 200 nm, respectively. The arrows indicate the location of the sample/glue interface.

high signals, i.e., height in the topography and measure for relative change in capacitance (ΔC_{rel}) in the SCM image. The bright line in the topography image indicates the border of the glue line which is slightly elevated due to a slower removal rate during polishing. The figure shows how topographical features and capacitance signals correlate. As to be expected, the SCM signal decreases in highly doped regions of the silicon and levels off at lower values for the lower dopant level of the bulk Si substrate. This allows us to pinpoint the location of the sample/glue interface in the SCM micrograph as indicated by the arrows; all valuable electrical SCM information is contained to the right of that point. Although no direct correlation is possible between signal output and absolute concentration, the micrographs clearly offer quantitative depth information.

This concept is more clearly shown in Fig. 2 which compares a line profile section, obtained from the software by cutting through the SCM micrograph, to a SIMS depth profile obtained on the same sample. In this figure, the sample surface is on the left-hand side. The origin of the SCM profile is at the sample/glue interface. The data show an excellent agreement for the total implant depth between the two techniques: The background of the SIMS measurement is at about 3×10^{14} atoms/cm^3, which also corresponds to the bulk dopant concentration of the p-type substrate. We can see from the SCM plot that it reaches its plateau at the same depth (top cursor at 1 μm) as the SIMS signal levels off. A further qualitative comparison shows that the rise in the SCM graph correlates to the maximum of the implant profile at 0.35 μm. Other features in this graph, such as the rise at the very beginning of the SCM graph and the SCM signals at depths shallower than the implant maximum, are discussed in Sec. IV, since these effects are related to resolution and sample/tip conditioning issues.

Figure 3 demonstrates the true capability of this technique for two-dimensional measurements. It shows results on a cross section of the NIST test structure, scanned over an area of 8 μm×8μm, which fully covered the implanted region

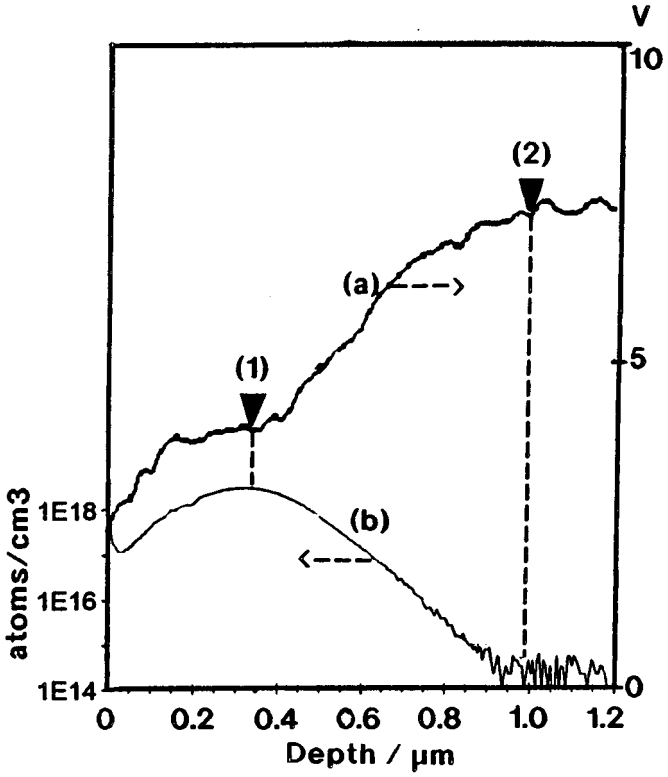

FIG. 2. Comparison of a single SCM line scan (a) from Fig. 1 and a SIMS depth profile (b) obtained on the same sample. The origin of the SCM profile is at the sample/glue interface. The cursors indicate the rise in the SCM data which coincides with the implant maximum at 0.35 μm (1) and the total implant depth at 1 μm (2).

between the 5 μm oxide lines. The sample surface is at the left-hand side. The thin oxide layers of 8 nm (in the opening) and 16 nm (oxide mask), respectively, are not resolved due to the limited point-to-point resolution in these images. However, the sample/glue interface can clearly be identified, and we can again correlate topographical and SCM features. The dark region in the SCM micrograph represents the relative ΔC changes in the implanted region.

Figure 4 compares SCM results from single line sections obtained in the center of the implanted area to a SIMS depth profile obtained from a large implanted region on the same sample. In agreement with Fig. 2, Fig. 4 shows an excellent agreement for total implant depth (0.75 μm) between the two techniques, as well as correlation of the SCM signal rise to implant maximum (0.23 μm).

Section IV discusses these results in light of the general capabilities and limitations of the SCM technique. An attempt is made for a two-dimensional correlation to SIMS data, and issues which affect the SCM sensitivity and resolution, signal quality, and the ability to measure heterojunctions are considered.

IV. DISCUSSION

A. Correlation to secondary ion mass spectrometry

We are aware of the differences between the two techniques with SIMS really measuring the total chemical dopant

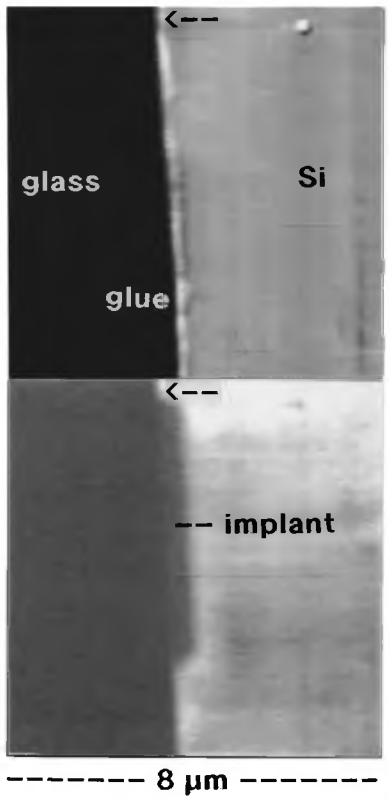

FIG. 3. Simultaneously acquired SCM data (bottom) and topographical data (top) of the cross-sectioned NIST test structure, scanned over an area of 8 μm×8 μm; signal ranges are 10 V and 40 nm, respectively. The arrows indicate the location of the sample/glue interface.

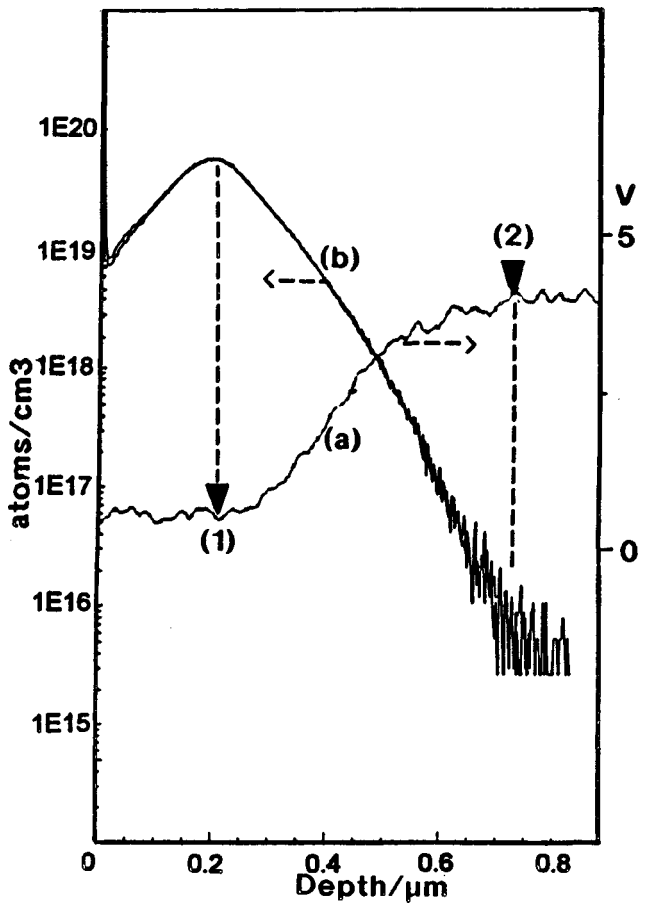

FIG. 4. Comparison of a single SCM line scan (a) in the center of the implant area of Fig. 3 and a SIMS depth profile (b) obtained from a large implanted region on the same sample. The SCM line scan starts at the sample/glue interface, the cursors indicate the rise coinciding with the implant maximum (1) and the total implant depth (2).

concentration, whereas the SCM technique captures only the electrically active carriers. However, we assume that in first approximation active carrier densities and chemical carrier concentrations are directly related. We further assume that a spatial correlation of SCM and SIMS signals is valid as long as it is done along a direction they have in common, which in these experiments is the direction vertical to the wafer surface. With this procedure, a particular SCM signal value at a certain depth can then be associated with a dopant concentration inferred from the SIMS profile at that same depth. In the next step, a two-dimensional dopant map is then obtained by assigning these dopant levels to the total two-dimensional SCM micrograph of the cross-sectioned test structure. This concept is illustrated in Fig. 5. It shows a SCM micrograph, displayed with an alternating black and white scale, which was obtained from an area of 1.15 μm×1.15 μm at the implant edge. It is oriented such that the interface is parallel to the y axis and coincides with the start of the SIMS profile. The contour lines have been labeled with the respective chemical dopant concentrations from the SIMS plot. The arrow indicates the location of the interface in the SCM data. Looking closely at the location of the interface, it becomes apparent that one or two contour lines seem to extend beyond the oxide/Si interface into the oxide. This might be attributable to possible fringe fields through the Si/oxide/glue interface or to artifacts caused by the size of electrically active portions of the tip. The latter could cause an electrical signal to be measured because a portion of the pyramidal tip sidewall is still located above the doped region, whereas the tip has already passed across the interface to the oxide layer. We expect that experiments with sharper tips will give more insight into these effects. Figure 5 also displays another noteworthy result. We can clearly see some contour lines at the top portion of the SCM image in an area between the actual implant stripes where we expected to only see a fairly constant low dopant level. Part of this is due to the limited lateral resolution, which at this low dopant region is only about 150 nm. In addition, we believe that, after checking back on the processing conditions, the masking during implant was not sufficient, and that the masked area got implanted to some extent in the near-surface region. This represents an interesting finding which could not have been obtained with any other technique for the given geometry.

Figure 5 represents the key result of our work. It demonstrates that the SCM technique can resolve carrier concentrations on cross sections in two dimensions with a single raster scan, using a standard sample preparation technique. The measurements are relatively easy to perform. From stability tests we found that as long as the feedback ensured stable imaging operation under constant load, no changes in the

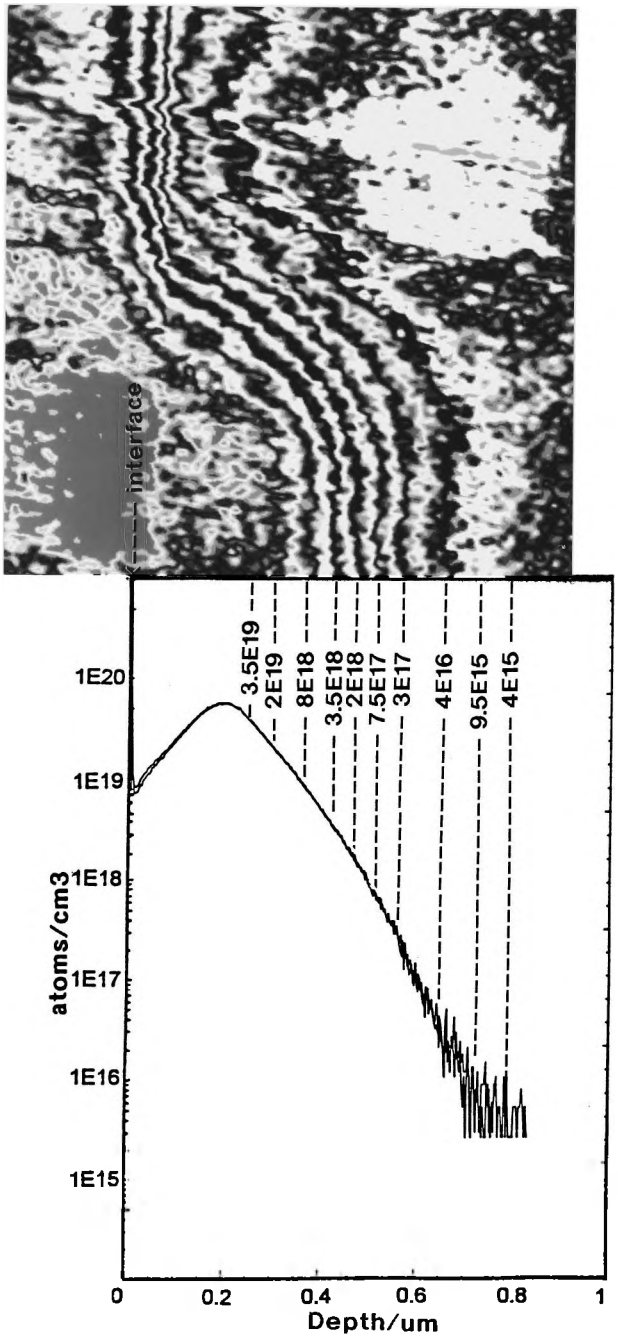

FIG. 5. Correlation of the SIMS data from Fig. 4 (bottom) to the two-dimensional SCM micrograph of the NIST test structure from a 1.15 μm $\times$1.15 μm area around the implant edge, displayed with an alternating black/white scale. The dark areas represent equi-ΔC_{rel} lines and are labeled with the respective chemical dopant concentrations from the SIMS profile.

SCM signals were observed. An excessively large contact load on the tip ($>10^{-5}$ N) was found to lead to a loss of signal of first capacitance and eventually also topography. With a normal operating load of about 5×10^{-7} N we have successfully scanned one such cross section for over 1 h obtaining several images without a change in signal. We also found in our experiments that changes leading to a loss in electrical signal were always rapid and occurred within a few scanning lines. We therefore believe that the most important

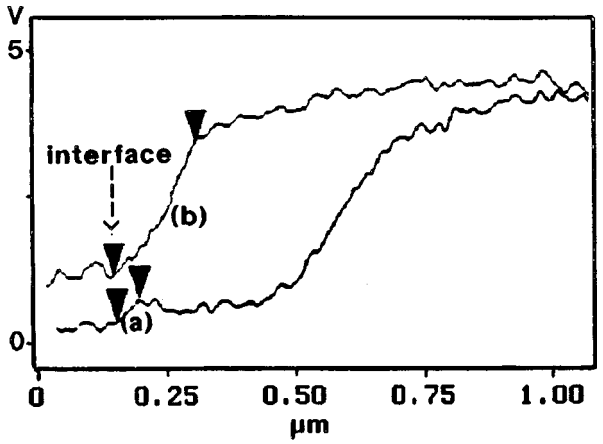

FIG. 6. SCM line scans, measured across the center of the oxide opening (a) and across the oxide line (b); the lateral extensions of the initial SCM signal increases at the sample surface measure 40 nm (a) and 150 nm (b), respectively, as indicated by cursor pairs.

limiting factor was the coating on the tip and that it failed due to delamination. This tip preparation procedure will need more perfection, but we expect that it could easily be improved.

B. Sensitivity and resolution

Overall noise levels can be estimated from SCM single line sections, such as in Fig. 4, to be mostly less than 10%. Refinement of the electrical setup should further improve this value. Sensitivities at particularly high or low dopant concentrations are best demonstrated using Figs. 4 and 2, as they show high peak dopant concentrations (Fig. 4) or low background doping (Fig. 2), respectively. Figure 4 shows the SCM signal starting to rise at the maximum of the SIMS depth profile, i.e., at a level of about 5×10^{19} atoms/cm^3. We see that the SCM signal output is almost twice as large at a level of 1×10^{19} atoms/cm^3. In a similar procedure, sensitivities at low dopant levels can be estimated from Fig. 2: We see that the SCM plot reaches its plateau at a depth of 1 μm, corresponding to about 3×10^{14} atoms/cm^3, as inferred from the SIMS profile. Levels of 1×10^{15}, 1×10^{16}, and 1×10^{17} atoms/cm^3 are found at SCM signals at about 93%, 85%, and 70%, respectively, of the maximum SCM signal in Fig. 2. Although these considerations demonstrate an acceptable dynamic range, the lateral resolution is largely sacrificed in the low dopant concentration range.

Estimates for this lateral resolution can be obtained from comparison of SCM line sections obtained from areas with greatly different carrier densities, but with the same probe tip. Figure 6 was obtained from Fig. 3 by plotting SCM line sections from a cut across the center of the oxide opening, much like the one in Fig. 2, and across the oxide line where the implant had been masked. We can see that the lower carrier density below the oxide mask results in a higher SCM signal at that depth, but the rise at the beginning of the SCM profile is significantly larger (150 nm) than for that at the oxide opening (40 nm). Measurements on other samples

have shown values as small as 20 nm. We interpret this as the "electrical tip diameter," because it is the combined effect of actual geometric tip diameter and carrier concentration. Due to the difference in carrier concentration, the applied ac bias results in a much larger depletion depth and interaction volume for the lower concentration. This results in a lateral "spread" of the signal and, consequently, a loss in lateral resolution. The same effect also becomes clear in Fig. 5, where the contour lines increase in width for measurements at higher depth, i.e., lower carrier densities. In our future work, we will, therefore, improve our setup to the feedback system recently developed by Huang, Williams, and Slinkman which allows a constant depletion depth to be maintained by varying the ac bias amplitude.[20]

C. Factors affecting signal quality

Several observations indicate that more work needs to be done to correctly interpret SCM signals close to an interface, i.e., within a tip radius off the interface. For example, Figs. 2 and 4 show that the SCM signal does not correlate well to the dopant concentration increase in the SIMS plot. As mentioned above, Fig. 5 seems to indicate some artifacts due to fringe field effects through the interface or tip artifacts introduced from the physical size of electrically active tip portions, i.e., the electrical tip diameter. We are planning to address these issues in several different ways. The use of sharper probe tips will improve on tip-related artifacts. Questions about fringe field effects and measurements of dopant levels close to an interface will be addressed through studies of blanket implants at varying levels with the same tip. Finally, we need to address sample passivation. Our current sample preparation uses a double-coated tip (Cr/Si oxide) to ensure proper insulating properties. Although this proves sufficient to avoid tunneling between tip and surface, a more repeatable tip and sample conditioning is desirable. A thin oxide on the sample of 100 Å or less would be best. It should be free of defects and contaminants, in other words, have uniform dielectric properties, which is not guaranteed in a native oxide. This requirement will be even more important for inverse modeling attempts as described in Ref. 20. We will examine sample passivation schemes with more scrutiny in future experiments. We are currently considering passivation through HF treatment, or in a low-temperature hydrogen furnace. Another possibility is the growth of low-temperature oxides, under UV light.[34,35]

D. Heterojunction considerations

As already mentioned in Sec. II, we have conducted a very limited number of experiments on samples with junctions to test the general applicability of the technique. It was found that our SCM setup clearly detects signal changes, indicating the location of the junction. However, Rodgers, Adderton, and Erickson have shown in a similar setup that $C-V$ curves acquired at the junction are not one dimensional in nature and demonstrate both n- and p-type behavior.[36] This is due to the three-dimensionality of the probe tip/sample geometry which causes the tip to interact with carriers on either side of the junction. Very recent measurements have shown a successful delineation when the device is electrically shorted across the junction. This effect will be further evaluated in future experiments.

V. CONCLUSIONS

As a key result of our work, we have successfully employed the SCM technique to measure two-dimensional maps of relative capacitance changes as a qualitative measure for carrier densities, when scanning cross sections of test structures with a two-dimensional dopant distribution. Two-dimensional quantitative data are easily obtained by correlation to SIMS profile data, acquired on the same sample. Correlation to structure geometry is obtained through simultaneously acquired AFM topography data. The fact that cross sections could be successfully measured is an additional advantage, since this is an important application for the semiconductor industry. Several crucial points of the technique have been identified which need to be addressed in the future. These include the development of a better sample passivation scheme, the study of SCM technique characteristics for measurements within a tip radius off the interface, the application of a bias feedback system, and a development of a three-dimensional model for the tip–surface interaction. We believe that this work represents an important milestone on the way to direct two-dimensional measurements of local carrier densities. Further experimentation, and especially modeling, are now necessary to achieve this goal.

ACKNOWLEDGMENTS

The authors wish to express their thanks to their respective departments for having made possible this cooperation between the four sites of Intel, NIST, University of Utah, and Digital Instruments. Professor L. Sadwick, University of Utah, has contributed many fruitful discussions in interpreting $C-V$ curves. One author (A. E.) would like to give thanks for the opportunity of summer internships with Intel Corporation which made this work possible. Special thanks go to Regina Campbell, Intel, for her patience, assistance, and "magic tips" to allow the authors to successfully prepare a variety of cross-sectioned samples, as well as to Jerry Hunter, Intel, and Clyve Jones, Philips Materials Analysis Laboratories, for measuring the SIMS depth profiles.

Certain trade names and company products are mentioned in the text or identified in an illustration in order to adequately specify the experimental procedure and equipment used. In no case does such identification imply recommendation or endorsement by the National Institute of Standards and Technology, nor does it imply that the products are necessarily the best available for the purpose.

[1]R. Subrahmanyan, J. Vac. Sci. Technol. B **10**, 358 (1992); Microelectron. Eng. **19**, 585 (1992).
[2]H. Cerva, in *Proceedings of the 1st International Workshop on the Measurement and Characterization of Ultra-Shallow Doping Profiles*, edited by C. M. Osburn and G. E. McGuire (AIP, New York, 1991), Vol. 2, p. 355.
[3]P. Roitman, J. Albers, and D. R. Meyers, J. Appl. Phys. **55**, 4436 (1984).

[4]S. H. Goodwin-Johansson, Y. Kim, M. Ray, and H. Z. Massoud, J. Vac. Sci. Technol. B **10**, 369 (1992).
[5]R. Chapman, M. Kellam, S. Goodwin-Johansson, J. Russ, and G. McGuire, J. Vac. Sci. Technol. B **10**, 502 (1992).
[6]T. Tagikami and M. Tanimoto, Appl. Phys. Lett. **58**, 2288 (1991).
[7]Y. Chiu, M. L. Reed, and T. E. Schlesinger, Appl. Phys. Lett. **60**, 1715 (1992).
[8]S. Kordic, E. J. vanLoenen, D. Dijkkamp, A. J. Hoeven, and H. K. Moraal, J. Vac. Sci. Technol. A **8**, 549 (1990); J. Vac. Sci. Technol. B **10**, 496 (1992).
[9]H. E. Hessel, U. Memmert, H. Cerva, and R. J. Behm, J. Vac. Sci. Technol. B **9**, 690 (1991).
[10]J. V. LaBrasca, R. C. Chapman, G. E. McGuire, and R. J. Nemanich, J. Vac. Sci. Technol. B **9**, 752 (1991).
[11]M. B. Johnson and J. M. Halbout, in Ref. 2, Vol. 2, p. 389.
[12]R. M. Feenstra and J. A. Stroscio, J. Vac. Sci. Technol. B **5**, 923 (1987).
[13]W. F. Tseng, J. A. Dagata, R. M. Silver, J. Fu, and J. R. Lowney, J. Vac. Sci. Technol. B **12**, 373 (1994).
[14]J. A. Dagata, W. Tseng, and R. M. Silver, J. Vac. Sci. Technol. A **11**, 1070 (1993).
[15]R. M. Silver, J. A. Dagata, and W. Tseng, J. Vac. Sci. Technol. B (to be published).
[16]C. K. Shih, J. Vac. Sci. Technol. B **11**, 1509 (1993); Appl. Phys. Lett. **64**, 493 (1994).
[17]O. Albrektsen, M. B. Johnson, R. M. Feenstra, and H. Salemink, Appl. Phys. Lett. **63**, 2923 (1993).
[18]H. Salemink and O. Albrektsen, J. Vac. Sci. Technol. B **9**, 779 (1991).
[19]Y. Huang and C. C. Williams, J. Vac. Sci. Technol. B **12**, 369 (1994).
[20]Y. Huang, C. C. Williams, and J. Slinkman, J. Vac. Sci. Technol. B (to be published).
[21]J. J. Kopanski, J. F. Marchiando, J. R. Lowney, and D. G. Seiler, NIST, Sematech, ASTM, E42.14, AVS; in Workshop Summary Report NISTIR No. 5550: *Industrial Applications of Scanned Probe Microscopy*, edited by J. A. Dagata, A. C. Diebold, C. K. Shih, and R. J. Colton (NTIS, Springfield, 1994), p. 63.
[22]Y. Huang and C. C. Williams, in *Proceedings of the 2nd International Workshop on the Measurement and Characterization of Ultra-Shallow Doping Profiles*, edited by R. Subrahmanyan, C. M. Osburn, and P. Rai-Choudhury (AIP, New York, 1993), Vol. 2, p. 286.
[23]D. W. Abraham, C. C. Williams, J. Slinkman, and H. K. Wickramasinghe, J. Vac. Sci. Technol. B **9**, 703 (1991).
[24]C. C. Williams, J. Slinkman, W. P. Hough, and H. K. Wickramasinghe, Appl. Phys. Lett. **55**, 1662 (1989).
[25]C. D. Bugg and P. J. King, J. Phys. E **21**, 147 (1988).
[26]P. DeWolf, T. Clarysse, W. Vandervorst, J. Snauwert, L. Hellemans, M. D'Olieslaeger, and D. Quahagens, J. Vac. Sci. Technol. B (to be published).
[27]T. Clarysse and W. Vandervorst, J. Vac. Sci. Technol. B **12**, 290 (1994).
[28]R. B. Marcus, in Ref. 21, p. 65.
[29]C. Shafai, D. J. Thomson, M. Simard-Normandin, G. Mattiussi, and P. J. Scanion, Appl. Phys. Lett. **64**, 342 (1994).
[30]M. Nonnenmacher, M. P. O'Boyle, and H. K. Wickramasinghe, Appl. Phys. Lett. **58**, 2921 (1991); Ultramicroscopy **42–44**, 268 (1992).
[31]G. Neubauer, M. L. A. Dass, and T. J. Johnson, Mater. Res. Soc. Symp. Proc. **265**, 283 (1992).
[32]J. R. Matey and J. Blanc, J. Appl. Phys. **47**, 1437 (1985).
[33]G. Neubauer and A. Erickson, in Ref. 21, p. 60.
[34]Y. Ishikawa, T. Shibamoto, T. Ushihara, and I. Nakamichi, Jpn. J. Appl. Phys. **30**, L661 (1991).
[35]A. Kazor and I. W. Boyd, Appl. Surf. Sci. **54**, 460 (1992).
[36]M. Rodgers, D. Adderton, and A. Erickson (unpublished).